

**Bicircular-laser-field-assisted electron-ion radiative recombination**S. Odžak<sup>1</sup> and D. B. Milošević<sup>1,2,3</sup><sup>1</sup>*Faculty of Science, University of Sarajevo, Zmaja od Bosne 35, 71000 Sarajevo, Bosnia and Herzegovina*<sup>2</sup>*Max-Born-Institut, Max-Born-Strasse 2a, 12489 Berlin, Germany*<sup>3</sup>*Academy of Sciences and Arts of Bosnia and Herzegovina, Bistrik 7, 71000 Sarajevo, Bosnia and Herzegovina*

(Received 20 August 2015; published 11 November 2015)

Electron-ion radiative recombination assisted by a bicircular laser field that consists of two circularly polarized fields counterrotating in the  $xy$  plane and having the frequencies  $r\omega$  and  $s\omega$ , which are integer multiples of the fundamental frequency  $\omega$ , is considered using the  $S$ -matrix theory. The energy and polarization of soft x rays generated in this process are analyzed as functions of the incident electron energy and incident electron angle with respect to the  $x$  axis. Numerical results for the process of direct recombination of electrons with  $\text{He}^+$  ionic targets are presented. Abrupt cutoffs of the plateau structures in the emitted x-ray energy spectra are explained by classical analysis. Simpler or more complex oscillatory structures in the spectrum may appear as a result of the interference of a different number of classical orbits. Symmetry analysis and the numerical results show that the x-ray power spectrum and ellipticity are invariant with respect to a rotation of the incident electron momentum by the angle  $2\pi/(r+s)$ . We have visualized this by presenting the logarithm of the differential power spectrum and polarization of the emitted x rays in false colors as functions of the incident electron angle and the x-ray energy. We have also shown that the change of the relative phase of the bicircular field is equivalent to the change of the incident electron angle. By controlling this relative phase it is possible to control the polarization of the emitted soft x rays.

DOI: [10.1103/PhysRevA.92.053416](https://doi.org/10.1103/PhysRevA.92.053416)

PACS number(s): 34.80.Qb, 34.80.Lx, 33.20.Xx, 32.30.Rj

**I. INTRODUCTION**

Over the past few decades the generation of coherent, extreme ultraviolet radiation and of soft x rays has been a topic of a great scientific and practical importance. Some of the atomic processes in which the production of high-energy photons is possible are high-order harmonic generation (HHG) (see, for example, the review articles in Refs. [1–4], and references therein), laser-assisted x-ray–atom scattering [5–7], laser-induced bremsstrahlung [8–12], and laser-assisted electron-ion recombination [13–24].

The process of electron-ion recombination is very important in plasma physics and astrophysics [25]. In the case of radiative recombination the energy is transferred from the free electron to a photon. By applying additional external laser field, the incident electron may exchange the energy with the laser field before it recombines with the target ion. As a result, a high-energy photon is emitted (see Ref. [2], and references therein). It should also be mentioned that the external laser field can cause a significant gain of the recombination yield, which may be important for the laser-assisted neutral antimatter formation [26]. The laser-induced enhancement of the recombination rate has also been observed in experiments with merged ion and electron beams (in ion storage rings) [27]. The effects of polarization on laser-induced electron-ion recombination in the electron cooler of the storage ring were considered in Ref. [28]. Multiphoton-assisted recombination was investigated experimentally in Ref. [29]. In the present paper we consider the process of direct laser-assisted recombination (LAR).

The atomic and molecular processes can be controlled by applying a bichromatic laser field and by varying the relative phase and the amplitudes of the field components (see the review article in Ref. [30], and references therein). For the LAR process the emitted-x-ray spectrum was analyzed as a function of the relative phase of linearly polarized bichromatic

field with frequencies  $\omega$  and  $2\omega$  in Ref. [16] and the possibility of the coherent phase control was confirmed. The dependence of the LAR energy spectra on the carrier-envelope phase of a few-cycle laser pulse was considered in Ref. [24]. In the present paper we consider electron-ion radiative recombination assisted by the so-called bicircular field. This field consists of two coplanar counterrotating circularly polarized fields having frequencies  $r\omega$  and  $s\omega$ , where  $r$  and  $s$  are arbitrary integers and  $\omega$  is the fundamental frequency (with the corresponding period  $T = 2\pi/\omega$ ), and relative phases  $\phi_r$  and  $\phi_s$ . We analyze how the LAR process can be controlled by changing the parameters of the bicircular field.

Very recently, HHG by a bicircular laser field has become a hot topic of research [31–38]. The reason is that the harmonics generated by the bicircular field are circularly polarized and as such they are a valuable tool for investigation of chirality-sensitive light-matter interactions. It should be mentioned that 20 years ago it was shown that the bicircular field is an efficient tool for HHG [39]. The theories of HHG by a bicircular field have shown that the emitted harmonics should be circularly polarized [40–44], but this was confirmed experimentally only recently [31]. Having in mind that HHG can be considered as a three-step process that consists of strong-field ionization followed by electron propagation and laser-assisted electron-parent ion recombination, it is clear that for a better understanding of HHG by a bicircular field, it is important to investigate LAR in a bicircular field. It should be mentioned that the three-step model of HHG was formulated in Ref. [45] and further elaborated in the context of the strong-field approximation [46] and a quasiclassical approach that includes the Coulomb correction [47]. There are many references related to this subject of which we mention [48] and the review articles in Refs. [1–4,49], and references therein. More recently, the photorecombination cross section of atoms was retrieved from HHG spectra [50]

using the so-called quantitative rescattering theory and the corresponding factorization formula (see the review article in Refs. [49,51] for a derivation of the factorization formula using time-dependent effective range theory). In addition, it should be mentioned that above-threshold ionization, a process that is inverse to the LAR, by a bicircular field was recently considered in Refs. [52,53].

The present paper is devoted to the investigation of electron-ion radiative recombination assisted by a bicircular laser field. These introductory remarks are followed by the quantum-mechanical theory based on the  $S$ -matrix formalism and on the classical analysis, which are presented in Sec. II. We have extended our previous theory so that it can be applied for an arbitrarily polarized laser field and to the polarization analysis of the emitted x rays. The corresponding symmetry analysis is relegated to the Appendix. Section III contains our numerical results. We first present the results for the differential power spectra and explain them using classical analysis. After that we consider the polarization properties of the emitted soft x rays and put all this in the context of dynamical symmetries. Finally, the conclusions are summarized in Sec. IV. The atomic system of units ( $\hbar = e = m_e = 4\pi\epsilon_0 = 1$ ) is used throughout the paper.

## II. THEORY

A theoretical description of the direct LAR process, based on the  $S$ -matrix formalism, was given in Ref. [15]. The incident electron having the momentum  $\mathbf{p}$  recombines with a positive ion and an atomic bound state of energy  $E_B < 0$  is formed. This process happens in the presence of a strong periodic laser field with the electric-field vector  $\mathbf{E}(t)$  and during this process an x-ray photon having the wave vector  $\mathbf{K}$ , frequency  $\omega_{\mathbf{K}}$ , and unit complex polarization vector  $\hat{\mathbf{e}}_{\mathbf{K}}$  is emitted. The LAR process is characterized by the differential power spectrum [15]

$$S(\mathbf{K}, \mathbf{p}) = \frac{p\omega_{\mathbf{K}}^4}{2\pi c^3} |T_n|^2, \quad (1)$$

where  $T_n = \mathbf{T}(\mathbf{K}, \mathbf{p}) \cdot \hat{\mathbf{e}}_{\mathbf{K}}^*$  is the  $T$ -matrix element. The number of photons  $n$  exchanged with the laser field is obtained from the energy conserving condition

$$n = (\omega_{\mathbf{K}} + E_B - E_p - U_p)/\omega, \quad (2)$$

where  $E_p = \mathbf{p}^2/2$ ,  $U_p = \int_0^T \mathbf{A}^2(t) dt / (2T)$  is the ponderomotive energy, and  $\mathbf{A}(t) = -\int^t \mathbf{E}(t') dt' = d\boldsymbol{\alpha}(t)/dt$ . In the length gauge and dipole approximation we have

$$\begin{aligned} \mathbf{T}(\mathbf{K}, \mathbf{p}) &= T_n \hat{\mathbf{e}}_{\mathbf{K}} = \int_0^T \frac{dt}{T} \langle \psi_B | \mathbf{r} e^{-i\mathbf{K}\cdot\mathbf{r}} | \mathbf{p} + \mathbf{A}(t) \rangle \\ &\times \exp \left\{ i(E_B + \omega_{\mathbf{K}})t - \frac{i}{2} \int^t dt' [\mathbf{p} + \mathbf{A}(t')]^2 \right\}, \end{aligned} \quad (3)$$

where  $|\psi_B\rangle$  is the atomic bound-state ket vector and  $|\mathbf{p}\rangle$  is a plane wave [such that  $\langle \mathbf{r} | \mathbf{p} \rangle = (2\pi)^{-3/2} \exp(i\mathbf{p} \cdot \mathbf{r})$ ].

In most papers about the LAR the polarization of the emitted-x-ray photons is not considered. In the general case it is elliptical [19]. Similarly to Refs. [35,41], we define

the degree of circular polarization  $\xi_{\mathbf{K}} = \text{Im}(2T_{nx}^* T_{ny}) / |T_n|^2$ , where we have assumed that the vector  $\mathbf{K}$  is along the  $z$  axis and that  $\mathbf{T}(\mathbf{K}, \mathbf{p}) = T_{nx} \hat{\mathbf{e}}_x + T_{ny} \hat{\mathbf{e}}_y$ , with  $\hat{\mathbf{e}}_x$  and  $\hat{\mathbf{e}}_y$  the real unit polarization vectors along the  $x$  and  $y$  axes, respectively. Then the ellipticity of the emitted x ray is given by

$$\epsilon_{\mathbf{K}} = \text{sgn}(\xi_{\mathbf{K}}) \left( \frac{1 - \sqrt{1 - \xi_{\mathbf{K}}^2}}{1 + \sqrt{1 - \xi_{\mathbf{K}}^2}} \right)^{1/2}. \quad (4)$$

The integral over the recombination time  $t$  in Eq. (3) can be solved numerically. In addition, a semiclassical analysis can be done using the stationarity condition that the first derivative over time of the action in the exponent in (3) is equal to zero, leading to the equation

$$\frac{1}{2}[\mathbf{p} + \mathbf{A}(t)]^2 = E_B + \omega_{\mathbf{K}}, \quad (5)$$

which expresses the energy-conserving condition at the recombination time  $t$ : The classical electron kinetic energy in the laser field at time  $t$  has to be equal to the energy of the ground state, into which the electron recombines, plus the emitted-x-ray energy. In this paper we will support our numerical results by a classical analysis for which  $E_B + \omega_{\mathbf{K}} > 0$  and Eq. (5) has real solutions.

We use a bichromatic circularly polarized field with coplanar counterrotating components having the angular frequencies  $r\omega$  and  $s\omega$ , which are integer multiples of the same fundamental frequency  $\omega$ . The corresponding electric-field vector in the  $xy$  plane is defined by [41–43]

$$\mathbf{E}(t) = \frac{i}{2} [E_r \hat{\mathbf{e}}_+ e^{-i(r\omega t + \phi_r)} + E_s \hat{\mathbf{e}}_- e^{-i(s\omega t + \phi_s)}] + \text{c.c.}, \quad (6)$$

where  $\hat{\mathbf{e}}_{\pm} = (\hat{\mathbf{e}}_x \pm i\hat{\mathbf{e}}_y)/\sqrt{2}$ . In Eq. (6)  $\phi_j$ ,  $E_j$ , and  $I_j = E_j^2$  are the phase, amplitude, and intensity of the  $j$ th field component of helicity  $h_j$  ( $h_r = 1$  and  $h_s = -1$ ). The components of the bicircular field (6) are given by

$$\begin{aligned} E_x(t) &= [E_r \sin(r\omega t + \phi_r) + E_s \sin(s\omega t + \phi_s)]/\sqrt{2}, \\ E_y(t) &= [-E_r \cos(r\omega t + \phi_r) + E_s \cos(s\omega t + \phi_s)]/\sqrt{2}. \end{aligned} \quad (7)$$

Defining  $A_r = E_r/(r\omega)$  and  $A_s = E_s/(s\omega)$ , for the ponderomotive energy we obtain  $U_p = (A_r^2 + A_s^2)/4$ . In Fig. 1 we present the normalized electric-field vector  $\mathbf{E}(t)$  and the pertinent normalized vector potential  $\mathbf{A}(t)$  for various combinations of  $(r, s) \in \{(1,2), (1,3), (1,4), (1,5), (2,3), (2,5)\}$ . The intensities of the field components are equal and the relative phases are set to zero.

The bicircular field  $\mathbf{E}(t)$  and the vectors  $\mathbf{A}(t)$  and  $\boldsymbol{\alpha}(t)$  obey the following dynamical symmetry: The rotation by the angle  $\alpha_j = -2\pi jr/(r+s)$  about the  $z$  axis is equivalent to the translation in time by  $\tau_j = jT/(r+s)$ , i.e.,

$$R_z(\alpha_j) \mathbf{E}(t) = \mathbf{E}(t + \tau_j), \quad (8)$$

where  $j$  is an integer, the diagonal matrix element of the rotation matrix  $R_z(\alpha_j)$  is  $\cos \alpha_j$ , and the off-diagonal elements are  $\pm \sin \alpha_j$ . This dynamical symmetry can be used to show that the differential power spectrum is invariant with respect to rotation about the  $z$  axis by the angle  $-\alpha_j/r$  (see the

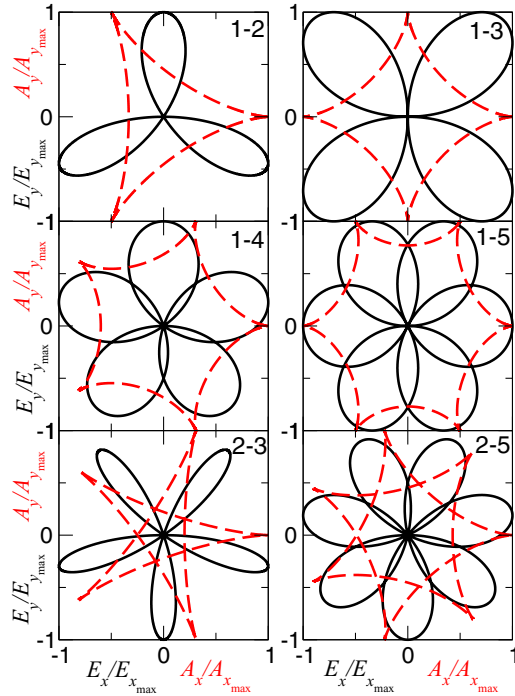


FIG. 1. (Color online) Normalized electric-field vector  $\mathbf{E}(t)$  (solid black lines) and vector potential  $\mathbf{A}(t)$  (dashed red lines) of the  $r\omega - s\omega$  bicircular laser field given by Eq. (7) for equal laser field component intensities and the relative phases  $\phi_r = \phi_s = 0$ , plotted for  $0 \leq t \leq T$ ,  $T = 2\pi/\omega$ . The electric-field vector starts from the point  $\mathbf{E}(0) = (0,0)$  and develops in the clockwise direction for  $t > 0$ , while the vector potential develops in the counterclockwise sense. The various panels depict the field for different combinations of the values of  $r$  and  $s$  as indicated in the upper right corners.

Appendix):

$$S\left(\mathbf{K}, R_z\left(\frac{2\pi j}{r+s}\right)\mathbf{p}\right) = S(\mathbf{K}, \mathbf{p}). \quad (9)$$

Here the vector  $\mathbf{K}$  is along the  $z$  axis, so  $R_z(-\alpha_j/r)\mathbf{K} = \mathbf{K}$ . The incident electron momentum is in the  $xy$  plane such that  $\mathbf{p} \cdot \hat{\mathbf{e}}_x = p \cos \theta$ . In addition, in the Appendix it is shown that the ellipticity  $\varepsilon_{\mathbf{K}}$  is also invariant with respect to the rotation by the angle  $2\pi j/(r+s)$  about the  $z$  axis.

### III. NUMERICAL RESULTS

In this section we present numerical results for direct recombination of electrons with  $\text{He}^+$  ions. We model the  $s$  ground-state wave function of the He atom by a linear combination of the Slater-type orbitals [54]. The energy of the bound state of the He atom is  $E_B = -24.59$  eV. We use a bicircular laser field defined by Eq. (6) with the fundamental wavelength of 800 nm and the same laser field component intensities  $I_r = I_s = 10^{15}$  W/cm<sup>2</sup>. The coordinate system is chosen in a such way that the electron momentum  $\mathbf{p}$  lies in the  $xy$  plane and the incident electron angle is  $\theta = \angle(\mathbf{p}, \hat{\mathbf{e}}_x)$ .

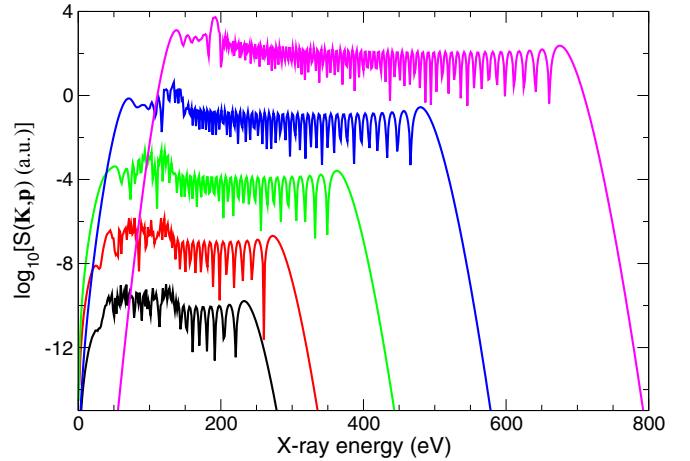


FIG. 2. (Color online) Logarithm of the differential power spectrum for the laser-assisted radiative recombination of electrons with  $\text{He}^+$  ions in the presence of the bicircular laser field (6) with the fundamental wavelength of 800 nm,  $I_r = I_s = 10^{15}$  W/cm<sup>2</sup>, and  $\phi_r = \phi_s = 0$  ( $r = 1$ ,  $s = 2$ ), as a function of the emitted x-ray energy  $\omega_{\mathbf{K}}$ . The incident electron energies for the curves from bottom to top are  $E_p = 10, 20, 50, 100$ , and  $200$  eV, respectively. The incident electron angle is  $\theta = 0^\circ$ . The ordinate of the bottom curve ( $E_p = 10$  eV) is in atomic units, while all other curves are shifted up by three orders of magnitude, consecutively.

#### A. Differential power spectrum and classical analysis

In Fig. 2 we present the differential power spectrum as a function of the emitted-x-ray energy for a bicircular laser field with  $r = 1$ ,  $s = 2$ , and  $\phi_r = \phi_s = 0$ , the incident electron angle  $\theta = 0^\circ$ , and the incident electron energy  $E_p = 10, 20, 50, 100$ , and  $200$  eV. All these results are presented on a logarithmic scale. The ordinate of the bottom curve ( $E_p = 10$  eV) is in atomic units and for a better presentation, all other curves are shifted up by three orders of magnitude, consecutively. Each of the energy spectra in Fig. 2 shows a plateau with an abrupt cutoff whose position shifts to higher photon energies when the incident electron energy increases. In addition, one can notice that for all presented curves characteristic simple or complex oscillatory structures appear.

Oscillatory structures and cutoff positions of the plateaus in the energy spectra can be explained by the classical analysis. The emitted-x-ray energy  $\omega_{\mathbf{K}}$  as a function of the recombination time  $t$ , obtained using Eq. (5), is presented in Fig. 3. The incident electron angle and energy are  $\theta = 0^\circ$  and  $E_p = 50$  eV, respectively, and  $(r,s) = (1,2)$ . All other laser and atomic parameters are set to the same values as in Fig. 2. The number of contributing classical orbits depends on the particular x-ray energy range that is clearly indicated in Fig. 3 by horizontal red dashed lines. The intersections of these horizontal lines and the curve  $\omega_{\mathbf{K}}(t)$  are denoted by the closed red circles. In the presented case, we have three different intervals of  $\omega_{\mathbf{K}}$  where only two or six solutions of Eq. (5) per optical cycle contribute. In other words, we have only two or six classical orbits per optical cycle that contribute to the spectrum. These intervals are indicated by I, II, and III. For  $\omega_{\mathbf{K}} \in [34.4, 87]$  eV (the region indicated by I) there are only two solutions of Eq. (5). This means that the main

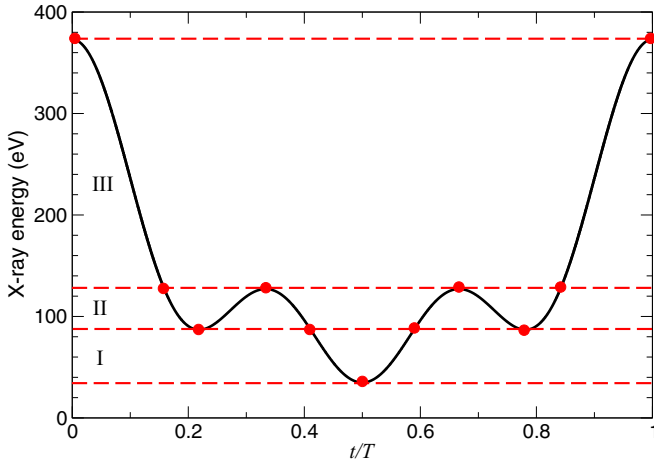


FIG. 3. (Color online) Classical analysis of the direct recombination solutions for the parameters of Fig. 2. The emitted x-ray energy  $\omega_{\mathbf{K}}$  is presented as a function of the recombination time  $t$ , expressed in units of  $T$ . The incident electron energy is  $E_p = 50$  eV.

contribution to the integral over time  $t$  in the  $T$ -matrix element, for a given emitted-x-ray energy  $\omega_{\mathbf{K}}$ , comes from two different times  $t_i$ ,  $i = 1, 2$ . The interference of these two contributions gives a simple interference structure. This is in accord with the numerical results presented in Fig. 2 [see the green (middle) curve and the corresponding above-mentioned interval of x-ray energies]. These solutions merge into one solution for  $t = 0.5T$ , which is indicated by the red closed circle. For the x-ray energy  $\omega_{\mathbf{K}} \in [87, 127]$  eV (the region indicated by II) six solutions of Eq. (5) contribute. The end points of this interval are also indicated by the red closed circles. The interference of these solutions gives a complicated structure and this is clearly visible in Fig. 2. For the x-ray energies  $\omega_{\mathbf{K}} \in [127, 373]$  eV (the region indicated by III), again only two solutions of Eq. (5) contribute with the corresponding simple interference structure. For the x-ray energies  $\omega_{\mathbf{K}}$  below 34.4 eV and above the cutoff value 373 eV there are no more real solutions.

In order to obtain stationary times that correspond to the extremal values of  $\omega_{\mathbf{K}}$  we have to solve equation obtained from the condition  $d\omega_{\mathbf{K}}/dt = 0$ . Using Eq. (5) we obtain

$$[\mathbf{p} + \mathbf{A}(t_m)] \cdot \mathbf{E}(t_m) = 0. \quad (10)$$

From the condition  $\mathbf{E}(t_m) = \mathbf{0}$  it follows that

$$t_m = \frac{T}{\pi(r+s)} \left( j\pi - \frac{\phi_r + \phi_s}{2} \right), \quad (11)$$

where  $0 \leq t_m \leq T$ . For the chosen parameters from Fig. 3 ( $\phi_r = \phi_s = 0$ ) we obtain four stationary points:  $t_1 = 0$ ,  $t_2 = T/3$ ,  $t_3 = 2T/3$ , and  $t_4 = T$ . These times correspond to the local ( $t_2$  and  $t_3$ ) and global ( $t_1$  and  $t_4$ ) maxima. This is in accord with the numerical results presented in Fig. 3. The other stationary times that correspond to the local and global minima can be obtained from the condition  $\mathbf{p} + \mathbf{A}(t_m) = \mathbf{0}$ . The positions of these minima depend on the incident electron angle and energy.

Inserting solutions of Eq. (10) into Eq. (5), we obtain the corresponding maxima and minima of  $\omega_{\mathbf{K}}$ . In such a way, inserting  $t_m$  given by Eq. (11) into Eq. (5), the cutoff position

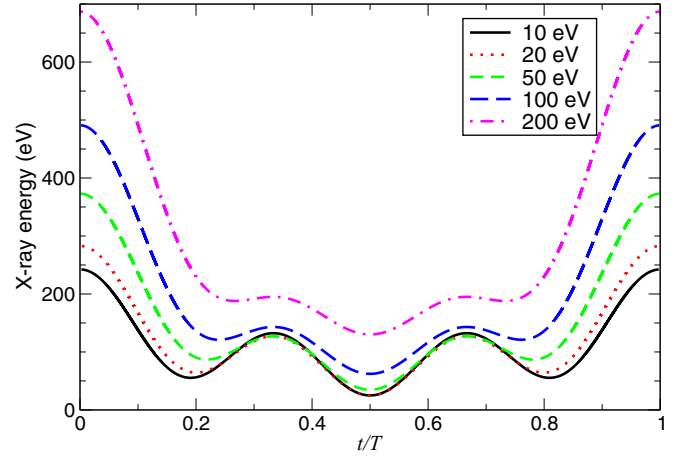


FIG. 4. (Color online) Classical analysis of the direct recombination solutions for the parameters of Fig. 2. The emitted x-ray energy  $\omega_{\mathbf{K}}$  is presented as a function of the recombination time  $t$ , expressed in units of  $T$ . The incident electron energy for each curve is indicated in the top right corner.

is determined by

$$\omega_{\mathbf{K}\max} = |E_B| + E_p + \frac{1}{2} \mathbf{A}^2(t_m) + \mathbf{p} \cdot \mathbf{A}(t_m). \quad (12)$$

Therefore, the cutoff position depends on the incident electron energy and angle as well as the phases of bicircular field. The increase of the electron energy leads to an increase of the cutoff position. This is in accord with the numerical results presented in Fig. 2.

In order to show the dependence of the width of the indicated regions (I–III) on the incident electron energy, in Fig. 4 we present the results obtained by solving Eq. (5) for the same parameters as in Fig. 2. The five incident electron energies are indicated in the top right corner. The widths of all three labeled regions change as functions of the incident electron energy. Thus, the interval of  $\omega_{\mathbf{K}}$  with the impact of two classical orbits (region I) becomes narrower when the incident electron energy increases. The same is valid for region II with the impact of six classical orbits. In contrast, the width of region III becomes narrower when the incident electron energy decreases. The reason for this is the decrease of the cutoff value with decreasing  $E_p$ . The highest maximum for each presented incident electron energy in Fig. 4 matches the cutoff energy of the plateau of the corresponding curve in Fig. 2. Comparing Figs. 2 and 4, we conclude that the results obtained by numerical integration [Eqs. (1)–(3)] agree very well with the estimates based on the classical analysis [Eq. (5)].

Another example of the LAR energy spectrum is presented in Fig. 5. The incident electron angle is now  $\theta = 180^\circ$ , while the other parameters are the same as in Fig. 2. From the numerical results presented in Figs. 2 and 5 we can see that the cutoff positions for all incident electron energies for  $\theta = 180^\circ$  are lower than those of the  $\theta = 0^\circ$  case.

In order to additionally explore oscillatory structures, the position of the cutoffs of the plateaus in the energy spectra, and the above-mentioned regions with the impact of different numbers of classical orbits on the spectrum, in Fig. 6 we present  $\omega_{\mathbf{K}}$  as a function of the recombination time  $t$  for

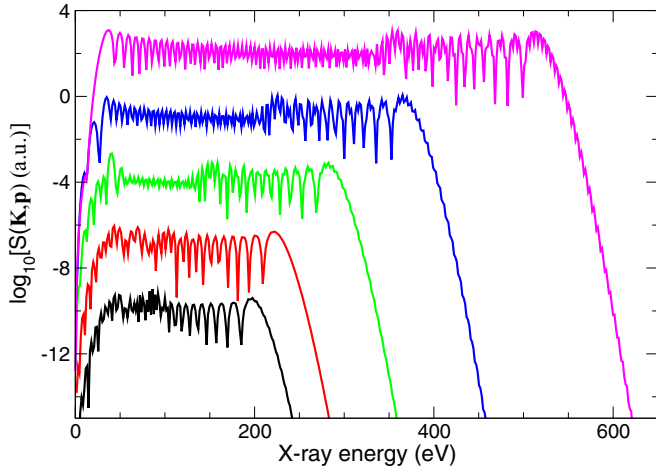


FIG. 5. (Color online) Same as in Fig. 2 but for  $\theta = 180^\circ$ .

$E_p = 50$  eV and  $\theta = 180^\circ$ . As in the case of the numerical results presented in Fig. 3, the number of solutions of Eq. (5) depends on the particular value of the x-ray energy. Unlike the case of the numerical results presented in Fig. 3, a region with the impact of four classical orbits appears (see region I). So, for  $\omega_K \in [25.5, 45]$  eV there are four solutions of Eq. (5). The corresponding interference structure becomes more complicated than the structure in the case where only two solutions interfere. With a further increase of the x-ray energy, for  $\omega_K \in [45, 144.2]$  eV (region II) only two classical orbits interfere. Finally, for  $\omega_K \in [144.2, 291]$  eV (region III), we again obtain the contribution of four solutions of Eq. (5). This leads to oscillations in the cutoff region. Below 25.5 eV and above the cutoff value 291 eV there are no more real solutions. Unlike the case of the numerical results presented in Fig. 3, the region with the impact of six classical orbits does not exist for the chosen parameters.

In Fig. 7 we present numerical results for  $\theta = 180^\circ$  and the same parameters as in Fig. 4 for five different incident electron energies indicated in the top right corner. The widths of all three above-mentioned regions also change as functions of the incident electron energy. So the interval of  $\omega_K$  with the impact

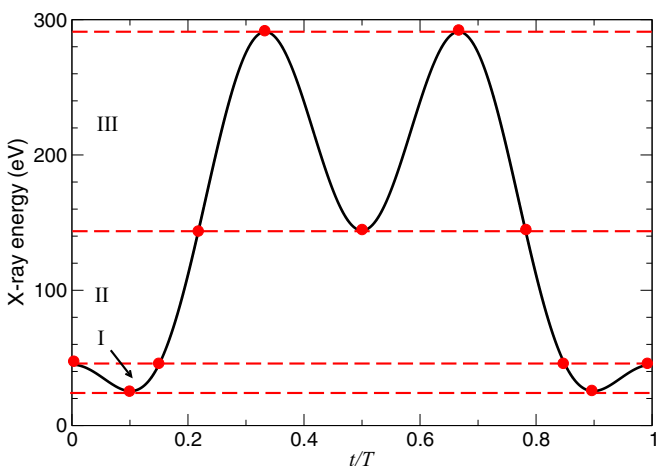


FIG. 6. (Color online) Same as in Fig. 3 but for  $\theta = 180^\circ$ .

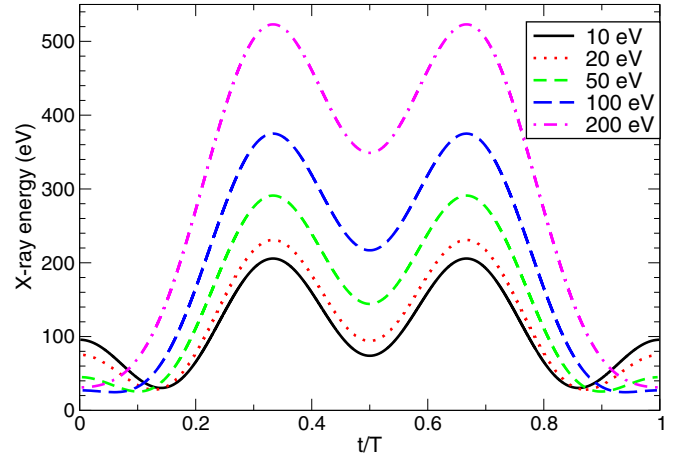


FIG. 7. (Color online) Same as in Fig. 4 but for  $\theta = 180^\circ$ .

of four classical orbits (region I) becomes narrower when the incident electron energy increases. In the case of  $E_p = 100$  and 200 eV this region almost disappears (see the blue long-dashed curve and magenta dot-dashed curve and the regions around  $t/T \in [0, 0.1]$  and  $t/T \in [0.9, 1]$ ). Region II with the impact of two classical orbits gradually disappears with the decrease of the incident electron energy. This region even completely disappears for  $E_p = 10$  eV (black solid curve). The reason is the increase of the x-ray energy for  $t/T$  around 0 and 1 with the decrease of the incident electron energy. The width of region III where four solutions contribute becomes wider when  $E_p$  increases. This is in accord with the numerical results presented in Fig. 5.

In order to obtain deeper insight into the regions that correspond to different numbers of solutions of Eq. (5), in Fig. 8 we present the differential power spectrum coded in false color, as a function of the incident electron angle (horizontal axis) and the x-ray energy (vertical axis). The laser and atomic parameters are the same as in Fig. 2 with  $E_p = 20$  eV. In Fig. 8 the regions with the impact of different numbers of solutions are clearly distinguishable. All these regions have conical-like

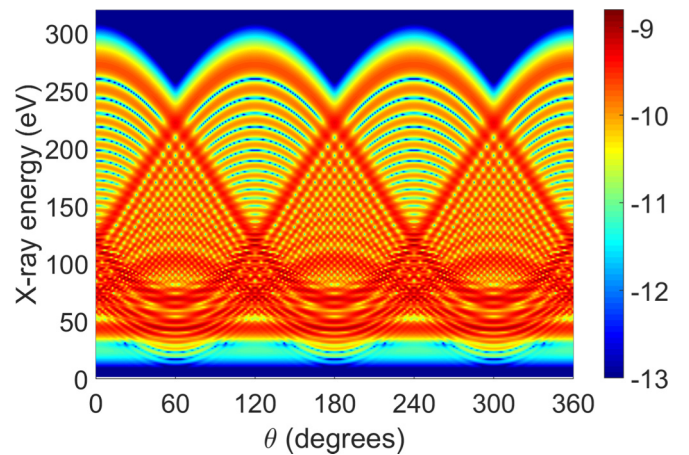


FIG. 8. (Color online) Logarithm of the differential power spectrum in false color as a function of the incident electron angle and the x-ray energy for  $E_p = 20$  eV and the same laser and atomic parameters as in Fig. 2.

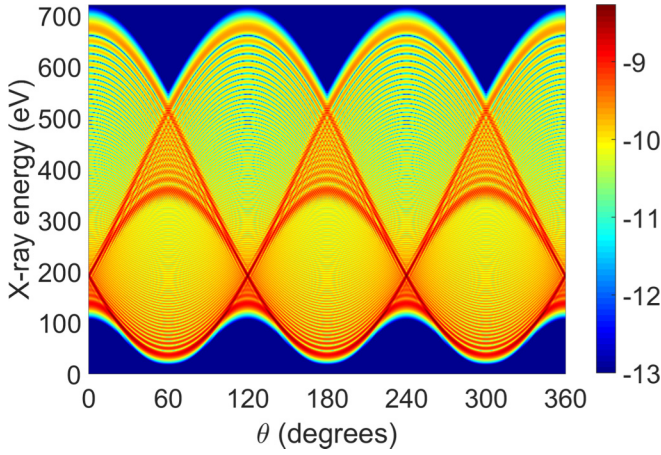


FIG. 9. (Color online) Same as in Fig. 8 but for  $E_p = 200$  eV.

or similar shapes and arise as a result of crossing oscillatory patterns in the spectrum. The regions where only two solutions contribute are less complex than in the case where four or six solutions of Eq. (5) contribute. Numerical results presented in Fig. 8 are in accord with the results presented in Figs. 2–7. The small region where only two solutions contribute to the spectrum for  $\theta = 180^\circ$  is visible in Fig. 8 as well as the existence of such a large region in the case of  $\theta = 0^\circ$ .

In Fig. 9 we present results analogous to those presented in Fig. 8 but for  $E_p = 200$  eV. The regions with the impact of different numbers of solutions of Eq. (5) are clearly visible. Again they are formed due to the interference of different periodically oscillatory structures. In this case the above-mentioned regions are clearly pronounced. Similar to the results presented in Fig. 8, the regions where only two solutions contribute for  $\theta = 0^\circ$  and  $180^\circ$  are clearly visible. This is in accord with the numerical results presented in Figs. 2–7 (see the magenta curves in these figures).

### B. Symmetry considerations and polarization of the emitted x rays

In order to additionally explore the symmetry of the LAR by bicircular field, in Fig. 10 we present the differential power spectrum for fixed incident electron energy  $E_p = 50$  eV and different combinations of  $(r, s)$ . The other laser and atomic parameters are the same as in Fig. 2. The symmetry effects are clearly visible for all chosen combinations of  $(r, s)$  presented in Fig. 10. They are in accord with Eq. (9) and the result of the Appendix. In addition, with the increase of  $r + s$ , regions of contributions of different numbers of solutions of Eq. (5) become smaller with a higher frequency of repetition. Since  $r + s$  is the same for the right panels of Fig. 10 [ $(r, s) = (1, 4)$  (top right panel) and  $(r, s) = (2, 3)$  (bottom right panel)] the

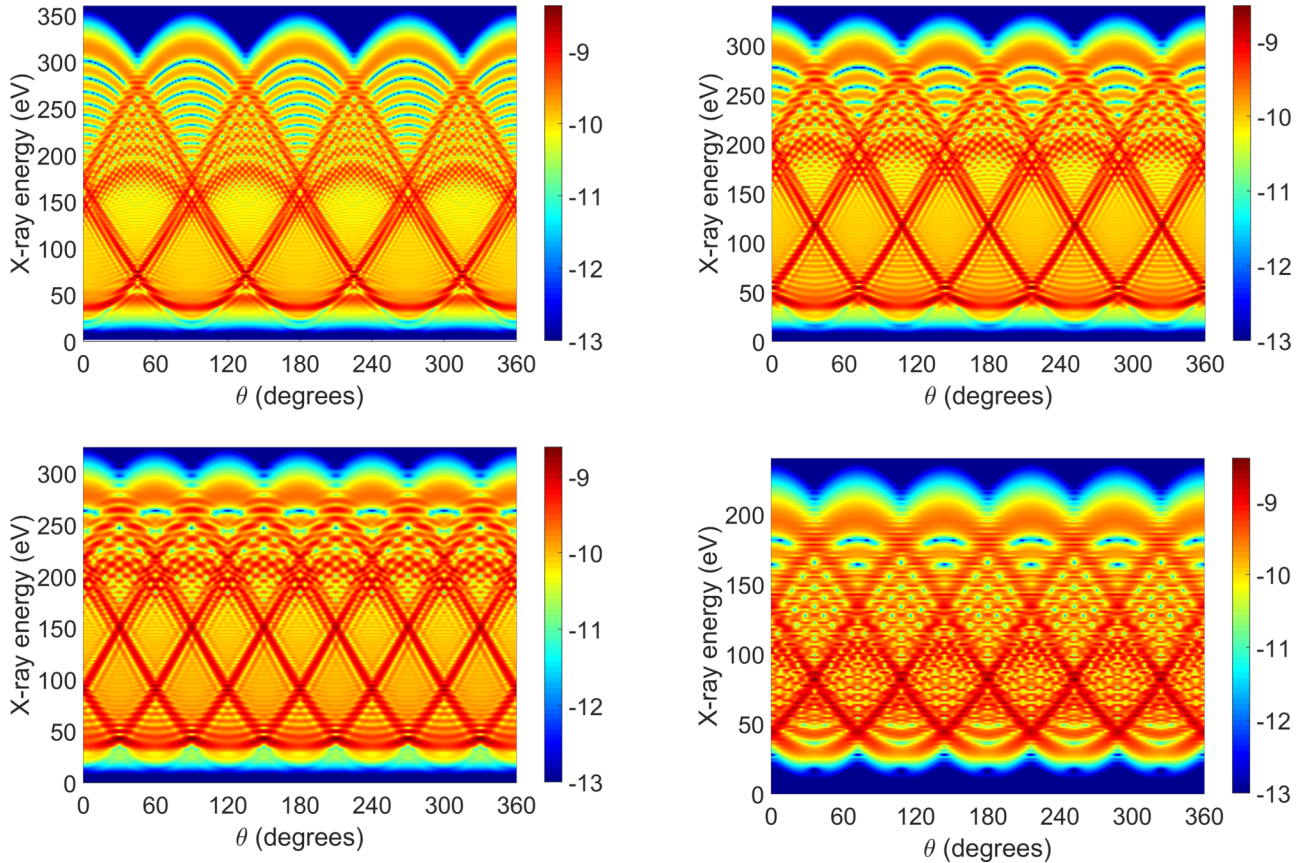


FIG. 10. (Color online) Logarithm of the differential power spectrum in false color as a function of the incident electron angle and the x-ray energy for fixed incident electron energy  $E_p = 50$  eV and different combinations  $(r, s)$ :  $(r, s) = (1, 3)$  (top left panel),  $(r, s) = (1, 4)$  (top right panel),  $(r, s) = (1, 5)$  (bottom left panel), and  $(r, s) = (2, 3)$  (bottom right panel). The other laser and atomic parameters are the same as in Fig. 2.

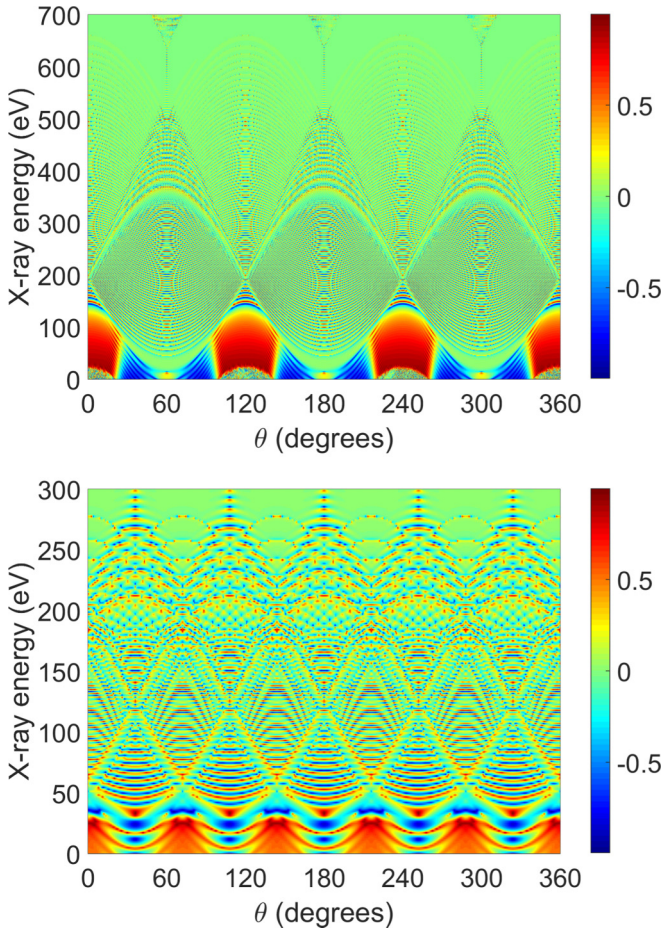


FIG. 11. (Color online) Ellipticity  $\varepsilon_{\mathbf{K}}$  in false color as a function of the incident electron angle and the x-ray energy for the same laser and atomic parameters as in Fig. 2 and for  $E_p = 200$  eV and  $(r,s) = (1,2)$  (top) and  $E_p = 50$  eV and  $(r,s) = (1,4)$  (bottom).

obtained oscillatory structures are very similar. Furthermore, a comparison of the panels from the first and second rows shows that the increase of the value of  $s$  implies more complex oscillatory structures.

The polarization of the emitted x rays satisfies similar symmetry properties. This is visible in Fig. 11, where the ellipticity is presented in false color as a function of the incident electron angle and the x-ray energy for  $E_p = 200$  eV for  $(r,s) = (1,2)$  and  $E_p = 50$  eV for  $(r,s) = (1,4)$ . In the region  $\theta \in [0, 2\pi/(r+s)]$  one can also notice the mirror symmetry  $\varepsilon_{\mathbf{K}}(\theta) = \varepsilon_{\mathbf{K}}[2\pi/(r+s) - \theta]$ . It is important that there are wide ranges of the incident electron angles and x-ray photon energies where the polarization of emitted x rays is close to circular. Such circular x rays can have important applications in x-ray magnetic circular dichroism spectroscopy [55] and for investigation of photoelectron circular dichroism in chiral molecules [56]. As an example, in Fig. 12 we show for  $E_p = 50$  eV,  $(r,s) = (1,2)$ , and  $\omega_{\mathbf{K}} = 109$  eV the dependence of the ellipticity  $\varepsilon_{\mathbf{K}}$  on the angle  $\theta$ . We see that for  $\theta = 55^\circ$  and  $65^\circ$  the ellipticity is  $\varepsilon_{\mathbf{K}} = -1$ .

One of the possible difficulties is how to change the incident electron angle in the experiment. We will now show that this problem can easily be solved. Namely, in the experiment one can fix the incident electron angle and investigate the angular

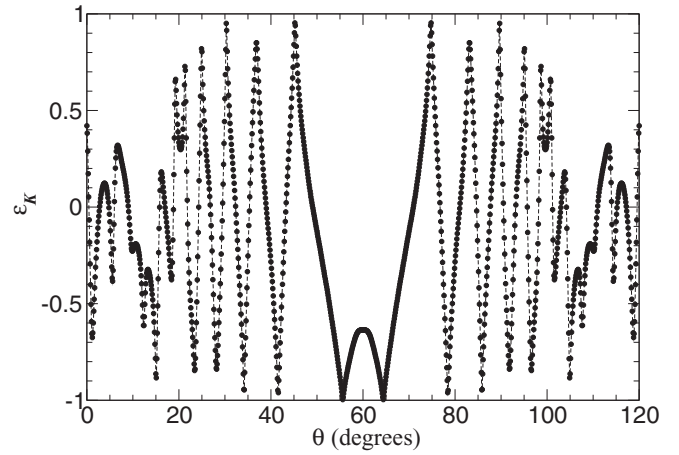


FIG. 12. Polarization  $\varepsilon_{\mathbf{K}}$  as a function of the incident electron angle  $\theta$  for  $E_p = 50$  eV,  $(r,s) = (1,2)$ , and the x-ray energy  $\omega_{\mathbf{K}} = 109$  eV. The other laser and atomic parameters are the same as in Fig. 2.

dependence of the emitted-x-ray energy and polarization by changing the phase  $\phi_r$  (or  $\phi_s$ ), which is much simpler. Let us prove this. In Fig. 13 we present our bicircular field for a fixed value of  $\phi_s = 0^\circ$  and for  $\phi_r = 0^\circ$  (black solid line) and  $\phi_r = 60^\circ$  (red dashed line). The impact of this change of the phase  $\phi_r$  from  $0^\circ$  to  $60^\circ$  is the rotation of bicircular field by the angle  $\alpha = 40^\circ$  in the  $xy$  plane as indicated in the figure. We have found a general connection between the phases  $\phi_r$  and  $\phi_s$  and the angle  $\alpha$ . For arbitrary (but fixed) values of  $\phi_s$ ,  $\phi_r$  and  $\alpha$  for arbitrary  $r$  and  $s$  are connected by the relation

$$\alpha = \frac{s\phi_r}{r+s}. \quad (13)$$

On the other hand, for an arbitrary (but fixed) value of  $\phi_r$ , the required relationship between  $\phi_s$  and  $\alpha$  is given by

$$\alpha = -\frac{\phi_s}{r+s}. \quad (14)$$

This means that a change of the phase  $\phi_r$  ( $\phi_s$ ) from zero to an arbitrary (but fixed) value  $\phi_r$  ( $\phi_s$ ) is equivalent to a

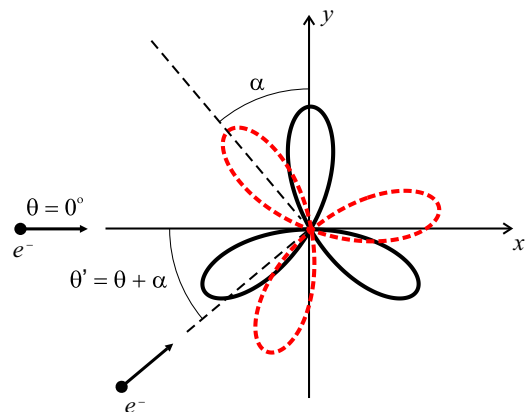


FIG. 13. (Color online) Bicircular  $\omega$ - $2\omega$  field for fixed phase  $\phi_s = 0^\circ$  and for two different values of the phase  $\phi_r$ ,  $\phi_r = 0^\circ$  (black solid line) and  $\phi_r = 60^\circ$  (red dashed line). The change of phase  $\phi_r$ , for fixed value of  $\phi_s$ , corresponds to the rotation field around the  $z$  axis by the angle  $\alpha$ .

change of the incident electron angle from  $\theta$  to  $\theta' = \theta + \alpha$ , as indicated in Fig. 13. This method can serve as a useful tool in experiments.

#### IV. CONCLUSION

The laser-assisted electron-ion recombination could be another potential source for generating coherent soft x rays and thus further information about this process will be useful in achieving this goal. The existing complementarity between the LAR process and the well-known HHG, especially in the case of a bicircular field, increases the importance of these investigations. In fact, the HHG is a process that can be explained using the three-step model, while the LAR is the third step of the HHG process. This implies the use of a similar theoretical formalism that is based on the  $S$ -matrix theory and on the classical analysis. By applying this theory, we have numerically investigated the emitted soft-x-ray spectrum as a function of the incoming electron energy  $E_p$  for different incident electron angles  $\theta$ . In our numerical calculations we have found that the maximum energy of the emitted x rays is higher for a higher incident electron energy. We have numerically investigated the dependence of the cutoff position on the angle  $\theta$  and explained our results using classical analysis.

For all chosen combination of  $(r, s)$  we have obtained a maximal cutoff energy of the differential power spectrum for the incident electron angles  $\theta = j2\pi/(r + s)$  ( $j = 0, 1, \dots, r + s$ ). We have also concluded that in the case of a bicircular laser field given by Eq. (6), simple or complex oscillatory structures in the spectrum may appear. They were observed and explained using our classical model. The reason for such oscillatory behavior is the interference of a smaller or larger number of classical orbits. The number of the contributing orbits strongly depends on the electron energy  $E_p$  and the chosen incident electron angle  $\theta$ . In the  $(r, s) = (1, 2)$  case we have concluded that there exist regions with the interference of two, four, or six classical orbits. In the general case, while analyzing the dependence of the spectra on the incident electron angle  $\theta$  for a fixed value of  $E_p$ , we have observed regions with less- or more-complex oscillatory structures. These regions may have a conical-like shape or some other shape that depends on the  $(r, s)$  combination used. The symmetry properties for the combinations  $(r, s) \in \{(1, 3), (1, 4), (1, 5), (2, 3)\}$  are also confirmed. We have shown that both the differential power spectrum and the ellipticity of the emitted x rays are invariant with respect to the rotation of the incident electron momentum by the angle  $2\pi/(r + s)$ . We have visualized this by presenting the logarithm of the differential power spectrum and polarization of the emitted x rays in false colors as functions of the incident electron angle and the x-ray energy.

Furthermore, we have shown that the polarization of the emitted x-ray photons can be close to circular for a particular incident electron angle interval. Such circularly polarized soft x rays can be used to study the chirality-sensitive properties of the light-matter interactions. Examples are photoelectron circular dichroism in chiral molecules [56] and x-ray magnetic circular dichroism spectroscopy [55]. The energy of these x rays can be larger than that of high-order harmonics generated by a bicircular field [33]. However, in comparison with the HHG, which is a laser-induced process in which the electron

recombines with its parent ion, it is more difficult to prepare electron and ion sources for LAR, so that one can expect that LAR is less efficient for producing soft x rays than HHG.

Laser-assisted recombination would allow for very clean experiments because one can specify the energy and the angle of the incident electron with very high precision (this is not so with the HHG process where recombination process is difficult to fully control since it is preceded by ionization and propagation, not to mention the macroscopic effects). In addition, we have found that by changing the relative phase of the bicircular field it is possible to rotate this field, which is equivalent to the rotation of the incident electron beam. Thus, it is possible to fix the incident electron angle and rotate the field by changing the relative phase in order to fulfill the condition for the generation of circularly polarized x rays, avoiding experimentally complicated rotation of the electron-beam source. It would also be interesting to explore the macroscopic effect on the LAR process. Focal-averaged spectra for LAR were presented in Ref. [20], but the phase matching, which is important for HHG [57,58], was not considered.

#### ACKNOWLEDGMENTS

We gratefully acknowledge support by the Federal Ministry of Education and Science, Bosnia and Herzegovina.

#### APPENDIX

In this Appendix we check the relation (9) and an analogous relation for the ellipticity  $\varepsilon_K$ . Denoting the vector rotated by the angle  $-\alpha_j = 2\pi jr/(r + s)$  around the  $z$  axis by the double prime, we have  $\mathbf{p}'' = R_z(-\alpha_j)\mathbf{p}$  and  $\mathbf{E}''(t + \tau_j) = \mathbf{E}(t)$ , where we have used Eq. (8). With this notation the integral  $\mathbf{T}(\mathbf{K}, \mathbf{p}'')$  [Eq. (3)] can be rewritten as

$$\begin{aligned} & \int_0^T \frac{dt}{T} \exp\left(i(E_B + \omega_{\mathbf{K}} - E_p)t - i\mathbf{p}'' \cdot \boldsymbol{\alpha}''(t + \tau_j) \right. \\ & \quad \left. - \frac{i}{2} \int^t dt'' \mathbf{A}''^2(t'' + \tau_j)\right) \\ & \quad \times \int d\mathbf{r} \psi_B^*(\mathbf{r}) \mathbf{r} e^{-i\mathbf{K} \cdot \mathbf{r}} (2\pi)^{-3/2} e^{i[\mathbf{p}'' + \mathbf{A}''(t + \tau_j)] \cdot \mathbf{r}}. \end{aligned} \quad (\text{A1})$$

The scalar product of two vectors is invariant with respect to rotations, so  $\mathbf{p}'' \cdot \boldsymbol{\alpha}''(t + \tau_j) = \mathbf{p} \cdot \boldsymbol{\alpha}(t + \tau_j)$ ,  $\mathbf{A}''^2(t'' + \tau_j) = \mathbf{A}^2(t'' + \tau_j)$ ,  $\mathbf{p}'' \cdot \mathbf{r} = [R_z(\alpha_j)R_z(-\alpha_j)\mathbf{p}] \cdot [R_z(\alpha_j)\mathbf{r}] = \mathbf{p} \cdot \mathbf{r}'$ , and  $\mathbf{A}''(t + \tau_j) \cdot \mathbf{r} = \mathbf{A}(t + \tau_j) \cdot \mathbf{r}'$ , where the prime denotes  $\mathbf{r}' = R_z(\alpha_j)\mathbf{r}$ . The vector  $\mathbf{K}$  is parallel to the  $z$  axis, so  $\mathbf{K} \cdot \mathbf{r} = \mathbf{K} \cdot \mathbf{r}'$ . We choose the quantization axis for the atomic bound state along the  $z$  axis and assume that  $\psi_B(\mathbf{r}) = \psi_B(\mathbf{r}')$ . Using  $\mathbf{r} = R_z(-\alpha_j)\mathbf{r}'$ ,  $d\mathbf{r} = d\mathbf{r}'$ , and the substitution  $t' = t + \tau_j$ , we get

$$\begin{aligned} \mathbf{T}(\mathbf{K}, \mathbf{p}'') &= e^{-i(E_B + \omega_{\mathbf{K}} - E_p)\tau_j} \int_{\tau_j}^{\tau_j + T} \frac{dt'}{T} e^{-i\mathbf{p} \cdot \boldsymbol{\alpha}(t')} \\ & \quad \times \exp\left(-\frac{i}{2} \int^t dt'' \mathbf{A}^2(t'') + i(E_B + \omega_{\mathbf{K}} - E_p)t'\right) \\ & \quad \times \int d\mathbf{r}' \psi_B^*(\mathbf{r}') R_z(-\alpha_j)\mathbf{r}' e^{-i\mathbf{K} \cdot \mathbf{r}'} \\ & \quad \times (2\pi)^{-3/2} e^{i[\mathbf{p} + \mathbf{A}(t')] \cdot \mathbf{r}'}. \end{aligned} \quad (\text{A2})$$

Since the integral in the interval  $[\tau_j, \tau_j + T]$  is the same as the integral in the interval  $[0, T]$ , we can rewrite the above relation as

$$\mathbf{T}(\mathbf{K}, \mathbf{p}'') = e^{-i(E_B + \omega_{\mathbf{K}} - E_p)\tau_j} R_z(-\alpha_j) \mathbf{T}(\mathbf{K}, \mathbf{p}). \quad (\text{A3})$$

The corresponding  $T$ -matrix element is  $\mathbf{T}(\mathbf{K}, \mathbf{p}'') \cdot \hat{\mathbf{e}}_{\mathbf{K}}''^* = \mathbf{T}''(\mathbf{K}, \mathbf{p}) \cdot \hat{\mathbf{e}}_{\mathbf{K}}''^* e^{-i(E_B + \omega_{\mathbf{K}} - E_p)\tau_j} = T_n e^{-i(E_B + \omega_{\mathbf{K}} - E_p)\tau_j}$ , so the differential power spectrum is invariant with respect to the rotation of  $\mathbf{p}$  by the angle  $-\alpha_j$ , i.e.,  $S(\mathbf{K}, \mathbf{p}'') = S(\mathbf{K}, \mathbf{p})$ . Since the invariance with respect to rotation by  $2\pi$  about the  $z$  axis is also valid, a more general rotational invariance with respect to the rotation by the angle  $2\pi[r(j + j') + sj']/(r + s)$  (where  $j$  and  $j'$  are integers) is satisfied. Then it can be

shown that for arbitrary  $r = 1, 2, \dots$  and  $s > r$  we have the invariance with respect to rotation by the angle  $2\pi j/(r + s)$ , i.e., the relation (9) is valid. This is clearly visible in Fig. 10.

Using the result (A3), it can also be shown that the degree of circular polarization  $\xi_{\mathbf{K}} = \text{Im}(2T_{nx}^* T_{ny})/|T_n|^2$  [and therefore the ellipticity  $\varepsilon_{\mathbf{K}}$ , Eq. (4)] is invariant with respect to the rotation by the angle  $-\alpha_j$  (and consequently by the angle  $-\alpha_j/r$ , as it is explained above in the case of the differential power spectrum). Namely, the phase factors in Eq. (A3) cancel and, after multiplication of the rotated matrix elements  $T_{nx}^*$  and  $T_{ny}$ , the imaginary part of the obtained result gives the factor  $\cos^2 \alpha_j + \sin^2 \alpha_j = 1$ .

- 
- [1] W. Becker, F. Grasbon, R. Kopold, D. B. Milošević, G. G. Paulus, and H. Walther, *Adv. At. Mol. Opt. Phys.* **48**, 35 (2002).
- [2] D. B. Milošević and F. Ehlotzky, *Adv. At. Mol. Opt. Phys.* **49**, 373 (2003).
- [3] F. Krausz and M. Ivanov, *Rev. Mod. Phys.* **81**, 163 (2009).
- [4] M. Kohler, T. Pfeifer, K. Hatsagortsyan, and C. Keitel, *Adv. At. Mol. Opt. Phys.* **61**, 159 (2012).
- [5] D. B. Milošević and F. Ehlotzky, *Phys. Rev. A* **58**, 2319 (1998).
- [6] D. B. Milošević and A. F. Starace, *Phys. Rev. Lett.* **81**, 5097 (1998); *Laser Phys.* **10**, 278 (2000).
- [7] D. B. Milošević and A. F. Starace, *J. Phys. B* **32**, 1831 (1999); *Phys. Rev. A* **60**, 3943 (1999).
- [8] R. V. Karapetyan and M. V. Fedorov, *Zh. Eksp. Teor. Fiz.* **75**, 816 (1978) [*Sov. Phys. JETP* **48**, 412 (1978)].
- [9] F. Zhou and L. Rosenberg, *Phys. Rev. A* **48**, 505 (1993).
- [10] F. Ehlotzky, A. Jaroń, and J. Z. Kamiński, *Phys. Rep.* **297**, 63 (1998).
- [11] M. Dondera and V. Florescu, *Radiat. Phys. Chem.* **75**, 1380 (2006).
- [12] A. N. Zheltukhin, A. V. Flegel, M. V. Frolov, N. L. Manakov, and A. F. Starace, *Phys. Rev. A* **89**, 023407 (2014); *J. Phys. B* **48**, 075202 (2015).
- [13] A. Jaroń, J. Z. Kamiński, and F. Ehlotzky, *Phys. Rev. A* **61**, 023404 (2000); **63**, 055401 (2001); *Laser Phys.* **11**, 174 (2001); *J. Phys. B* **34**, 1221 (2001).
- [14] M. Y. Kuchiev and V. N. Ostrovsky, *Phys. Rev. A* **61**, 033414 (2000); *J. Phys. B* **34**, 405 (2001).
- [15] D. B. Milošević and F. Ehlotzky, *Phys. Rev. A* **65**, 042504 (2002).
- [16] D. B. Milošević and F. Ehlotzky, *J. Mod. Opt.* **50**, 657 (2003).
- [17] C. Leone, S. Bivona, R. Burlon, and G. Ferrante, *Phys. Rev. A* **66**, 051403(R) (2002); S. Bivona, R. Burlon, G. Ferrante, and C. Leone, *J. Opt. Soc. Am. B* **22**, 2076 (2005); *Opt. Express* **14**, 3715 (2006); S. Bivona, R. Burlon, and C. Leone, *Laser Phys. Lett.* **4**, 44 (2007).
- [18] S. X. Hu and L. A. Collins, *Phys. Rev. A* **70**, 013407 (2004); **70**, 035401 (2004).
- [19] S. Bivona, G. Bonanno, R. Burlon, and C. Leone, *Phys. Rev. A* **76**, 031402(R) (2007).
- [20] A. Čerkić and D. B. Milošević, *Phys. Rev. A* **75**, 013412 (2007); *Laser Phys.* **19**, 783 (2009).
- [21] G. Shchedrin and A. Volberg, *J. Phys. A* **44**, 245301 (2011).
- [22] A. N. Zheltukhin, N. L. Manakov, A. V. Flegel, and M. V. Frolov, *Pis'ma Zh. Eksp. Teor. Fiz.* **94**, 641 (2011) [*JETP Lett.* **94**, 599 (2011)].
- [23] A. N. Zheltukhin, A. V. Flegel, M. V. Frolov, N. L. Manakov, and A. F. Starace, *J. Phys. B* **45**, 081001 (2012).
- [24] A. Čerkić and D. B. Milošević, *Phys. Rev. A* **88**, 023414 (2013).
- [25] Y. Hahn, *Rep. Prog. Phys.* **60**, 691 (1997).
- [26] M. L. Rogelstad, F. B. Yousif, T. J. Morgan, and J. B. A. Mitchell, *J. Phys. B* **30**, 3913 (1997); C. Wesdorp, F. Robicheaux, and L. D. Noordam, *Phys. Rev. Lett.* **84**, 3799 (2000); G. Gabrielse, *Adv. At. Mol. Opt. Phys.* **50**, 155 (2005).
- [27] U. Schramm, J. Berger, M. Grieser, D. Habs, E. Jaeschke, G. Kilgus, D. Schwalm, A. Wolf, R. Neumann, and R. Schuch, *Phys. Rev. Lett.* **67**, 22 (1991); A. Scrinzi, N. Elander, and A. Wolf, *Z. Phys. D* **34**, 185 (1995); U. Schramm, T. Schüssler, D. Habs, D. Schwalm, and A. Wolf, *Hyperfine Interact.* **99**, 309 (1996); U. Schramm, A. Wolf, T. Schübler, D. Habs, D. Schwalm, O. Uwira, J. Linkemann, and A. Müller, *ibid.* **108**, 273 (1997).
- [28] T. Mohamed, G. Andler, M. Fogle, E. Justiniano, S. Madzunkov, and R. Schuch, *Phys. Rev. A* **83**, 032702 (2011).
- [29] E. S. Shuman, R. R. Jones, and T. F. Gallagher, *Phys. Rev. Lett.* **101**, 263001 (2008); K. R. Overstreet, R. R. Jones, and T. F. Gallagher, *ibid.* **106**, 033002 (2011).
- [30] F. Ehlotzky, *Phys. Rep.* **345**, 175 (2001).
- [31] A. Fleischer, O. Kfir, T. Diskin, P. Sidorenko, and O. Cohen, *Nat. Photon.* **8**, 543 (2014).
- [32] E. Pisanty and M. Ivanov, *Nat. Photon.* **8**, 501 (2014); E. Pisanty, S. Sukiasyan, and M. Ivanov, *Phys. Rev. A* **90**, 043829 (2014).
- [33] O. Kfir, P. Grychtol, E. Turgut, R. Knut, D. Zusin, D. Popmintchev, T. Popmintchev, H. Nembach, J. M. Shaw, A. Fleischer, H. Kapteyn, M. Murnane, and O. Cohen, *Nat. Photon.* **9**, 99 (2015).
- [34] D. B. Milošević, *Opt. Lett.* **40**, 2381 (2015).
- [35] D. B. Milošević, *J. Phys. B* **48**, 171001 (2015).
- [36] D. D. Hickstein, F. J. Dollar, P. Grychtol, J. L. Ellis, R. Knut, C. Hernández-García, D. Zusin, C. Gentry, J. M. Shaw, T. Fan, K. M. Dorney, A. Becker, A. Jaroń-Becker, H. C. Kapteyn, M. M. Murnane, and C. G. Durfee, *Nat. Photonics* **9**, 743 (2015).
- [37] D. B. Milošević, *Phys. Rev. A* **92**, 043827 (2015).
- [38] T. Fan *et al.*, *Proc. Natl. Acad. Sci. (USA)* **112** (2015), doi:10.1073/pnas.1519666112.

- [39] H. Eichmann, A. Egbert, S. Nolte, C. Momma, B. Wellegehausen, W. Becker, S. Long, and J. K. McIver, *Phys. Rev. A* **51**, R3414 (1995).
- [40] S. Long, W. Becker, and J. K. McIver, *Phys. Rev. A* **52**, 2262 (1995).
- [41] D. B. Milošević, W. Becker, and R. Kopold, *Phys. Rev. A* **61**, 063403 (2000).
- [42] D. B. Milošević and W. Sandner, *Opt. Lett.* **25**, 1532 (2000); D. B. Milošević, W. Becker, R. Kopold, and W. Sandner, *Laser Phys.* **11**, 165 (2001).
- [43] D. B. Milošević, W. Becker, and R. Kopold, in *Atoms, Molecules and Quantum Dots in Laser Fields: Fundamental Processes*, edited by N. Bloembergen, N. Rahman, and A. Rizzo (Società Italiana di Fisica, Bologna, 2001), Vol. 71, pp. 239–252.
- [44] D. B. Milošević and W. Becker, *Phys. Rev. A* **62**, 011403(R) (2000); *J. Mod. Opt.* **52**, 233 (2005).
- [45] P. B. Corkum, *Phys. Rev. Lett.* **71**, 1994 (1993).
- [46] M. Lewenstein, P. Balcou, M. Y. Ivanov, A. L’Huillier, and P. B. Corkum, *Phys. Rev. A* **49**, 2117 (1994).
- [47] M. Y. Ivanov, T. Brabec, and N. Burnett, *Phys. Rev. A* **54**, 742 (1996).
- [48] M. Y. Kuchiev and V. N. Ostrovsky, *J. Phys. B* **32**, L189 (1999); *Phys. Rev. A* **60**, 3111 (1999).
- [49] C. D. Lin, A. T. Le, Z. Chen, T. Morishita, and R. Lucchese, *J. Phys. B* **43**, 122001 (2010).
- [50] T. Morishita, A. T. Le, Z. Chen, and C. D. Lin, *Phys. Rev. Lett.* **100**, 013903 (2008); S. Minemoto, T. Umegaki, Y. Oguchi, T. Morishita, A. T. Le, S. Watanabe, and H. Sakai, *Phys. Rev. A* **78**, 061402(R) (2008).
- [51] M. V. Frolov, N. L. Manakov, T. S. Sarantseva, and A. F. Starace, *J. Phys. B* **42**, 035601 (2009); *Phys. Rev. A* **83**, 043416 (2011).
- [52] E. Hasović, D. B. Milošević, and W. Becker, *Laser Phys. Lett.* **3**, 200 (2006); A. Kramo, E. Hasović, D. B. Milošević, and W. Becker, *ibid.* **4**, 279 (2007); E. Hasović, A. Kramo, and D. B. Milošević, *Eur. Phys. J. Spec. Top.* **160**, 205 (2008).
- [53] C. A. Mancuso, D. D. Hickstein, P. Grychtol, R. Knut, O. Kfir, X. M. Tong, F. Dollar, D. Zusin, M. Gopalakrishnan, C. Gentry, E. Turgut, J. L. Ellis, M.-C. Chen, A. Fleischer, O. Cohen, H. C. Kapteyn, and M. M. Murnane, *Phys. Rev. A* **91**, 031402(R) (2015).
- [54] A. A. Radzig and B. M. Smirnov, *Reference Data on Atoms, Molecules and Ions* (Springer, Berlin, 1985).
- [55] J. Stöhr, Y. Wu, B. D. Hermsmeier, M. G. Samant, G. R. Harp, S. Koranda, D. Dunham, and B. P. Tonner, *Science* **259**, 658 (1993); *Magnetism and Synchrotron Radiation: New Trends*, edited by E. Beaurepaire, H. Bulou, F. Scheurer, and J. P. Kappler (Springer, Heidelberg, 2010).
- [56] N. Böwering, T. Lischke, B. Schmidtke, N. Müller, T. Khalil, and U. Heinzmann, *Phys. Rev. Lett.* **86**, 1187 (2001); M. H. M. Janssen and I. Powis, *Phys. Chem. Chem. Phys.* **16**, 856 (2014).
- [57] P. Salières, A. L’Huillier, P. Antoine, and M. Lewenstein, *Adv. At. Mol. Opt. Phys.* **41**, 83 (1999).
- [58] T. Brabec and F. Krausz, *Rev. Mod. Phys.* **72**, 545 (2000).